Low-Temperature De-alloying and Unique Self-filling Interface Optimization Mechanism of Layered Silicon for Enhanced Lithium Storage

Wanling Ji[a], Minghuang Li[a], Yutong Nong[a], Jie Luo[a], Xinglong Liang[a], Xiaowei Wang[a]*, Lei Ming[a], Xing Ou[a], Jiafeng Zhang[a]*, Bao Zhang[a], Xuwang Fu[b], Lei Dong[b], Jianmin Feng[b]*, Ji Liang [c]*

[a.] *National Engineering Laboratory for High-Efficiency Recovery of Refractory Nonferrous Metals, School of Metallurgy and Environment, Central South University, Changsha 410083, PR China. Email: yjyzjf@csu.edu.cn. (J-F. Zhang)*

[b.] *College of Physics and Materials Science, Tianjin Normal University, No 393 Bin Shui West Road, Xiqing District, Tianjin 300387, China. E-mail: jmfeng@tjnu.edu.cn*

[c.] *School of Materials Science and Engineering, Tianjin University, China. E-mail: liangji@tju.edu.cn*

Table of contents

1. Vapor-Dealloying Preparation of Layered Silicon (L-Si)

Sample preparation. Mix the raw materials ammonium chloride (NH_4Cl) and calcium silicate ($CaSi_2$) evenly, and then heat them in a tube furnace to 300°C. $CaSi_2$ is used as a silicon source, and NH_4Cl is thermally decomposed into HCl gas and NH_3 gas. An argon gas stream is passed through a tube furnace at a flow rate of 100 ml/min. Under these conditions, HCl gas will react with $CaSi_2$ to form $CaCl_2$ and layered silicon. The as-prepared product was washed by pure water to remove $CaCl_2$, and layered silicon was obtained.

Materials Characterization. SEM observations and EDS analysis (SEM, TDCLS-8010, Hitachi Japan) is conducted as follows: the as-prepared product is dispersed in ethanol and dipped onto conductive tape as the analysis sample. In the same way, the as-prepared product ethanol solution is dropped copper grids coating with carbon film for TEM observation and EDX analysis (TEM, Talos F200X, FEI, US). The structure of the as-prepared products is analyzed by X-ray diffraction (XRD, D8 Advance, Bruker, German) and Raman spectroscopy (Horiba Jobin Yvon, LabRAM HR800, 17 mW, 514 nm, He-Ne laser), respectively. The surface chemistry of L-Si is analyzed by X-ray photoelectronic spectroscopy (XPS, Perkin-Elmer, PHI-1600, US).

2. The Application of L-Si for Lithium Storage

L-Si, acetylene carbon, carboxymethyl cellulose (CMC, dispersed in deionized water) are mixed as a weight percent of 7:2:1. Then the slurry is coated on Cu foil by a blade and dried at 90°C in a vacuum oven. The electrodes are punched into 12 mm disks for battery assembling. The counter electrode is a disk of lithium metal, and the separator is Celgard 2400. The electrolyte is 1 M $LiPF_6$ dissolved in a mixture of diethyl carbonate and ethylene carbonate (1:1 in volume) with 30% (volume ratio) Fluoroethylene carbonate additives. The assembly of the coin type half-cells is carried out in a glove box whose contents of H_2O and O_2 are less than 0.1 ppm. The working potential ranges from 0.01 to 3.0 V.

Cyclic Voltammetry (CV) analysis is carried out with a Princeton electrochemical workstation. Galvanostatic charge/discharge testing are conducted in the voltage range of 0.01-3.0 V (vs.Li/Li^+) using a LAND multichannel battery test system.

3. Cyclic Voltammetry (CV)

The electrochemical behavior of the L-Si towards Li storage has been further investigated using cyclic voltammetry (CV). The CV curves under various scanning rates from 0.2 to 1.0 mV s^{-1}

display similar but higher cathodic/anodic peaks intensity during lithiation/delithiation processes with the increase of scanning rates (**Fig. S5a, b, c**). Generally speaking, the lithium-ion storage mechanism includes battery behavior and pseudocapacitive behavior, which are controlled by diffusion and adsorption processes, respectively. The presence of pseudocapacitive behavior during the charging and discharging process can be calculated using the following formula:

$i = av^b (0.5 \leq b \leq 1)$

$logi = blogv + loga$

where *a* is a constant, *i* is peak current, and *v* is scan rate. If the *b* value is 0.5, the electrode material exhibits battery behavior and is controlled by the diffusion process. If the *b* value is 1.0, the electrode material exhibits pseudocapacitive behavior, which is controlled by the adsorption process. If the *b* value is between 0.5 and 1.0, the electrode material exhibits battery behavior and pseudocapacitive behavior. As shown in **Fig. S5d**, the calculated *b* value of the L-Si anode is 0.94, indicating that the L-Si anode is a lithium storage mechanism dominated by pseudocapacitive behavior.

Calculate the specific contribution ratio of pseudocapacitive behavior and battery behavior at a specific scanning speed using the following formula:

$i = k_1 v + k_2 v^{1/2}$

or

$$\frac{i}{v^{\frac{1}{2}}} = k_1 v^{1/2} + k_2$$

where k_1, k_2 are constants. At a given potential, the terms $k_1 v$ and $k_2 v^{1/2}$ represent the current response due to the capacitive process and diffusion-controlled faradaic process, respectively. The k_1 and k_2 can be calculated by plotting $i/v^{1/2}$ vs. $v^{1/2}$, thus the fraction of the charge from the capacitive process and diffusion-controlled process could be determined.

As shown in **Fig. S5e**, the capacitive process contribution of L-Si anode is 81.1% and the diffusion process contributes 18.9% of the total capacity, respectively. Contribution ratios between the two processes under different scan rates were also quantified.

Fig. S5f shows that the capacitive current ratio increased gradually with the increase of scanning rates, from 84% at 0.2 mV s^{-1} to 92% at 1.0 mV s^{-1}. The high ratio capacitive lithium storage contribution of L-Si indicates the adsorption and migration lithium storage mechanism.

4. Supporting Figures

Figure S1.

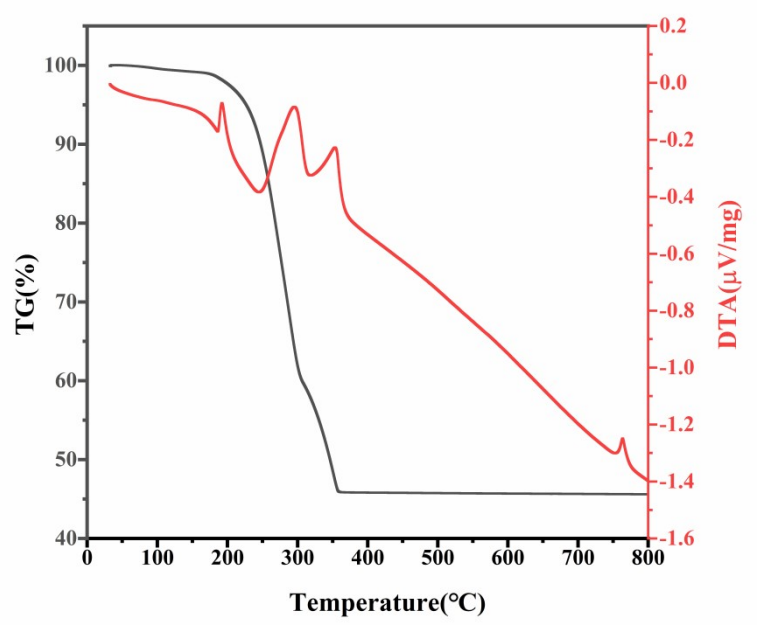

Figure S2.

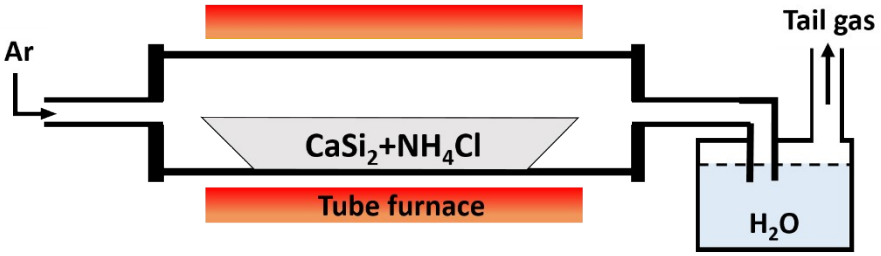

The synthesis equipment diagram of layered silicon is shown in Figure S2, where the thermal decomposition of NH_4Cl and the dealloying of $CaSi_2$ are carried out simultaneously in a tube furnace. The decomposition products of NH_4Cl are HCl and NH_3, among which HCl and $CaSi_2$ undergo dealloying reaction. Excess or unreacted HCl, and another decomposition product NH_3 will travel with an Ar flow to the tail gas treatment device, which is a simple device filled with water. The reason why the exhaust treatment device is so simple is that the gases HCl, NH_3, and even the by-product $CaCl_2$ generated in this process can be easily absorbed by water.

Figure S3.

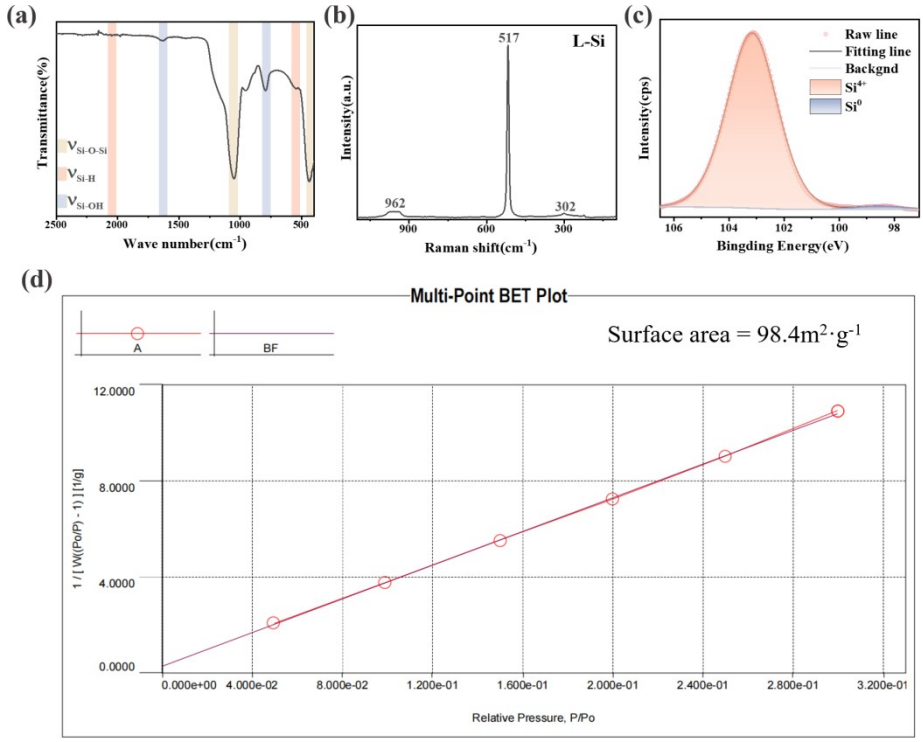

Surface composition analysis of the product L-Si was performed using various techniques (Figure S3). The FTIR spectrum (Figure S3a) reveals Si-H stretching vibrations at 2100 cm^{-1} and 540 cm^{-1}, as well as a Si-OH bending vibration at 1645 cm^{-1}. Additionally, a stretching vibration signal for Si-O-Si is observed at 1050 cm^{-1}.[15, 16] The presence of these signals is attributed to two factors: first, the exposure of the material to water during the impurity removal process, which leads to the formation of Si-O-Si bonds; and second, the high specific surface area of the layered silicon material (98.4 m^2/g, Figure S3d), which promotes substantial oxygen adsorption. This is corroborated by the strong Si^{4+} signal in the Si 2p XPS spectrum (Figure S3c).[9] Further analysis using Raman spectroscopy (Figure S3b) identified three characteristic silicon peaks at 302 cm^{-1}, 517 cm^{-1}, and 962 cm^{-1}, confirming the successful synthesis of the silicon material.[17]

Figure S4.

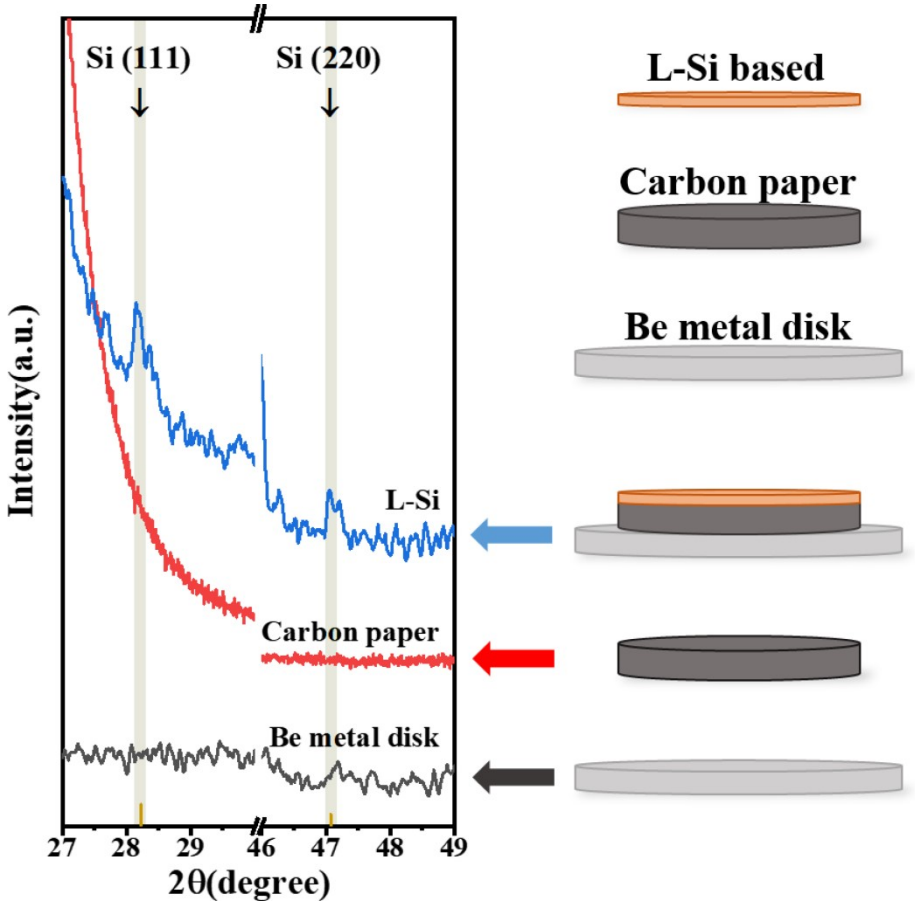

Figure S5.

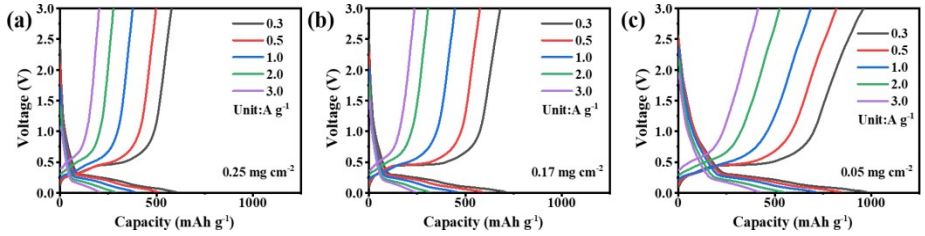

At a current density of 3.0 A g^{-1}, electrodes with areal densities of 0.25, 0.17, and 0.05 mg cm^{-2} exhibited reversible capacities of 207.74, 242.50, and 424.57 mAh g^{-1}, respectively (Figure S5). After 1200 cycles at 0.5 A g^{-1}, the L-Si electrode with an areal density of 0.05 mg cm^{-2} retained a high capacity of 1497.70 mAh g^{-1} with minimal degradation, demonstrating superior cycling performance compared to electrodes with higher areal densities of 0.25 mg cm^{-2} (400.00 mAh g^{-1}) and 0.17 mg cm^{-2} (491.08 mAh g^{-1}) (Figure 3e). These results suggest that the thickness of the layered silicon material during coating significantly impacts its electrochemical performance, likely due to the material's higher hardness and suboptimal contact with the current collector. This will be further investigated in subsequent cross-sectional SEM analyses. Reducing the areal density of L-Si electrodes markedly enhances their rate capability and cycling stability.

Figure S6.

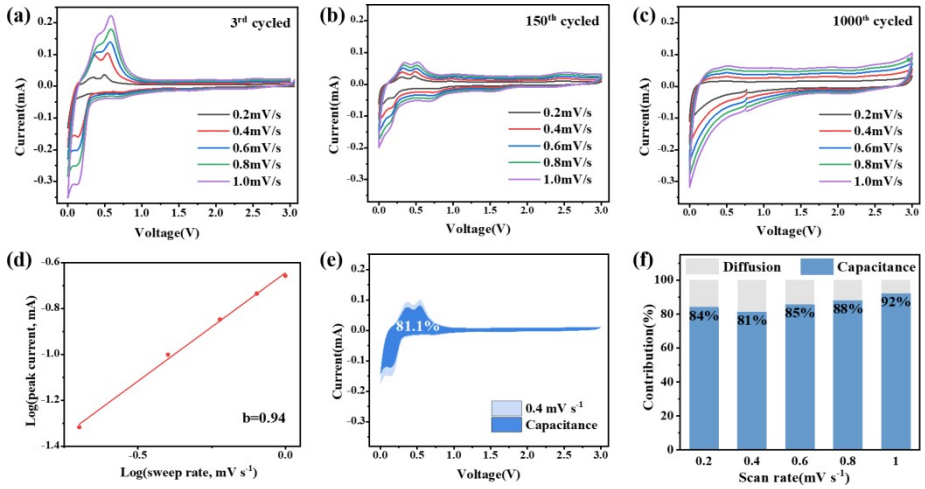

Figure S7.

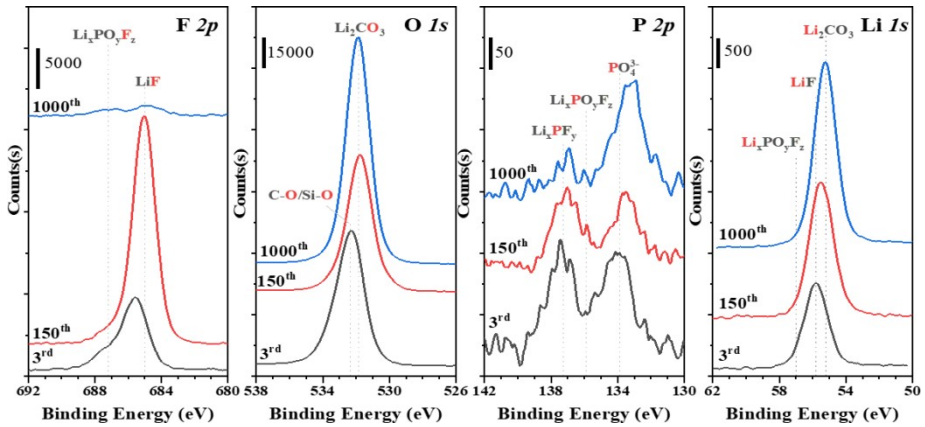

Figure S8.

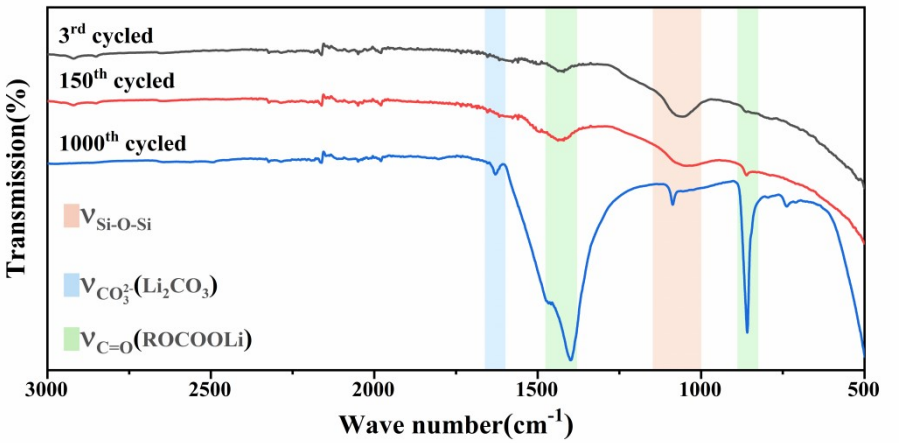

Figure S9.

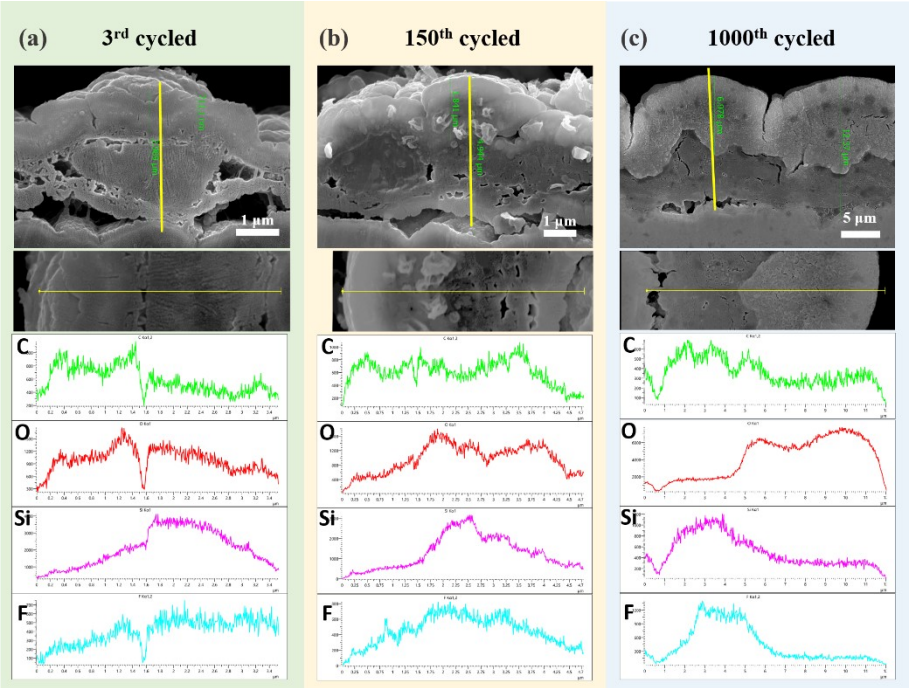

From the SEM images and line scan data of the electrode cross-section after 3, 150, and 1000 cycles (Figure S9), it can be analyzed that the lighter surface layer contains SEI film with C and O elements, while the darker interior is silicon (Si). As cycling progresses, the SEI film thickness increases, which aligns with XPS results. This thickening of the SEI film makes it harder to detect Si signals on the electrode surface in later cycles. Specifically, the thickness of the electrode after 3 cycles is 2.99μm, of which the thickness of the SEI film is only 711.1nm. At this stage, a layered structure of Si can be observed, and there are numerous voids in the electrode. By 150 cycles, the contact between the active material and the current collector becomes worse due to the volume expansion of the Si material. The thickness of the electrode increases to 4.94μm, and the SEI film thickness is 1.84μm at this stage. In addition, the EDS line scan results show that the C element becomes more evenly distributed inside the electrode. The thickness of the electrode increased to 12.37μm, and the SEI film thickness was 6.98μm after 1000 cycles. Although the thickness of the electrode has increased significantly at this stage, the large number of voids have disappeared, and the contact between the active material and the current collector has become very tight.

Figure S10.

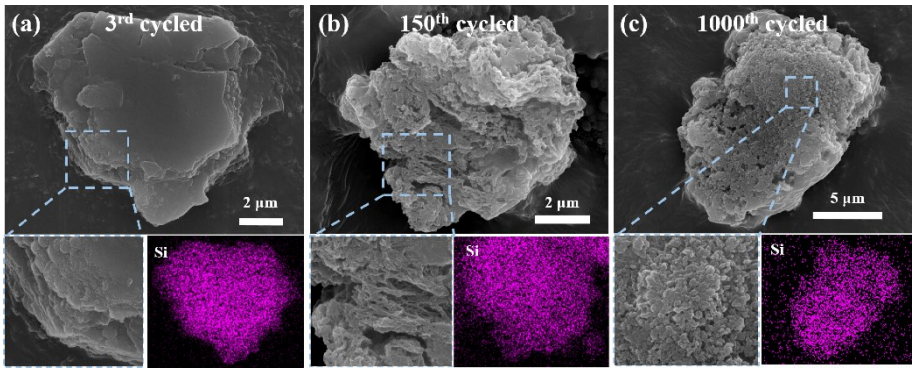

Furthermore, SEM characterization and EDS analysis were performed on the L-Si negative electrode material particles at each cycle stage (Figure S10). It can be observed that the Si in the electrode material after 3 cycles is a tightly layered structure, while at 150 cycles, the tightly stacked layered silicon transforms into sheet-like silicon with fluffy folds. After 1000 cycles, the silicon observed is composed of many small fragments aggregated, and no layered or sheet-like structure can be observed. At this stage, it can be seen that the layered silicon has broken into small fragments and is tightly cross-linked with various components of the electrode, as shown in the TEM image (Figure 4e).